CONSTRUCTION AND VALIDATION OF AN ANALYSIS TOOL CHAIN FOR ROTORCRAFT ACTIVE NOISE REDUCTION

Yasutada Tanabe, Shigeru Saito
e-mail: tan@chofu.jaxa.jp
JAXA (JAPAN)

Hideaki Sugawara
Ryoyu Systems, Co., Ltd. (JAPAN)

Abstract

This paper presents the construction and validation of a multi-disciplinary analysis chain based on high-fidelity CFD methods for the evaluation of active noise reduction devices. The active devices on the rotor blade which can be handled in current version of the code include the HHC, active flap, active tab and active twist. An all speed scheme was incorporated in the CFD solver to improve the accuracy of the flow prediction in the blade root and other areas with low air speeds. The natural frequencies and modes of a blade are treated as coupled bending with torsion modes uncoupled. The deformation of a blade is described using the mode decomposition method and is loosely coupled with the CFD solver, with the periodicity of the blade rotation presupposed. Trim adjustment in the rotor controls is also rendered in the CSD routine in order to match up with the target thrust and moments. The noise generated by the rotor is then predicted based on the Ffowcs-Williams and Hawking's equations using the integral method in Farassat Formulation 1. Validation of the analysis tools are performed with comparison to HART-II experimental data.

1. INTRODUCTION

Noise has been regarded as one of the serious problems for helicopter along with the cost and comfortableness. Operations are restricted in the urban area because of the noise concerns especially during night time which limits the utility of public service helicopters, such as emergency medical services which are called Doctor-Heli in Japan from the hospital based heli-pads. Noise from the helicopter sometime becomes a problem for the rescue activities on ground after a disastrous earthquake for example. Although quieter helicopters such as with NOTAR design are used more frequently for EMS, helicopters are still viewed as a noisy flying machine by most people. Revolutionary methods to reduce the helicopter noise remarkably are required and active control of the rotor blade is considered as one of the most promising approaches.

Various active control devices have been proposed and tested as shown in Figure 1. Between them, active flap has been tested most extensively while other devices such as active tab and active twist are proposed with better effects or specific advantages. Several full-scale rotor blades with active flaps have been manufactured and tested in the wind-tunnels and during flights. Significant noise reduction capability has been reported especially during descent flight where the noise caused by the Blade-Vortex Interaction (BVI) is dominant. However, in most cases, because of the complexity of the flow field and significance of the flow/structure coupling effect on the noise generation, the prediction and experimental results do not match well enough using the traditional comprehensive analysis software based on the lifting line theories. To build up an accurate and efficient high fidelity CFD-based analysis toolset for noise reduction design is still one of the urgent needs of the industry.

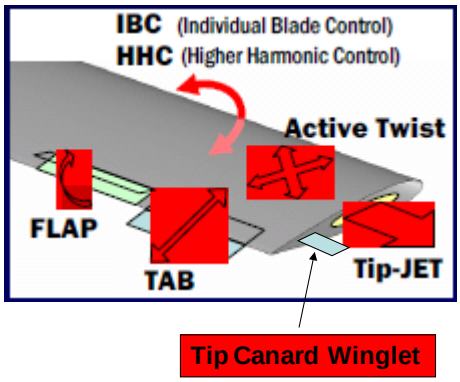

Figure 1: Various active control devices

An analysis tool chain has been constructed at JAXA [1] as shown in Figure 1. In the first step, the natural frequencies and modes of the rotating blade is calculated based on the structural properties of the blade and the operating conditions of the rotor. A code named as *rMode* is developed to obtain the

natural frequencies and modes required as inputs for CFD/CSD coupling analyses, which can also carry out the so-called fan-plot analysis and is useful for structural design of a blade to avoid vibrational resonance. The core of the multi-disciplinary analysis tool chain is the code named *rFlow3D/JANUS* which performs coupling CFD/CSD/Trim analyses based on a moving overlapped grid approach [2]. The *JANUS* code [3] combines an unstructured grid solver (*TAS-code*) [4] for the flowfield around the fuselage with the *rFlow3D* structured grid solvers for the blades and the background rectilinear grids. The deformation of a blade is described using the Ritz's mode decomposition method and is loosely coupled with the CFD solver, with the periodicity of the blade rotation presupposed. A numerically iterative solution to the Houbolt and Brooks' equation [5] based on coupled flapwise and chordwise bending and uncoupled torsion modes is found to improve the accuracy of the elastic deformations and more flexible to handle blade design changes, such as the location of sectional center of gravity compared to the solutions based on full coupled mode shapes where the formulations are simpler. Trim adjustment in the rotor controls is also rendered in the CSD routine in order to match up with the target thrust and moments. Finally, after a periodically converged solution of the flowfield together with the blade deformation is obtained, the noise generated by the rotor is then predicted based on the Ffowcs-Williams and Hawking's equations using the integral method in Farassat Formulation 1 [6] with the code named *rNoise*.

The airloads, elastic deformation and noise prediction accuracies are demonstrated based on HART-II test cases. Prediction accuracy of the BVI noise level is shown to be improved with computation grid refinement.

2. NUMERICAL APPROACHES

2.1. Analysis tool chain for helicopter noise

An analysis tool chain has been constructed as shown in Fig. 2. In the first step, the natural frequencies and modes of the rotating blade is calculated based on the structural properties of the blade and the operating conditions of the rotor. A code named as *rMode* is developed in JAXA which can carry out the so-called fan-plot analysis and is useful for the structural design of a blade to avoid vibration resonance.

The natural frequencies and mode shapes for a given rotating speed as outputs from *rMode* are used as inputs to the CFD/CSD coupling analysis solver *rFlow3D/JANUS*. The *rFlow3D* code [7] is solely developed in JAXA which can manipulate structural grids only, while the *JANUS* code [3] combines the unstructured grid solver TAS-code [4] developed in Tohoku University with the *rFlow3D* code which extends the ability of solving the realistic complex rotorcraft geometries while retaining high resolution of the rotor wakes.

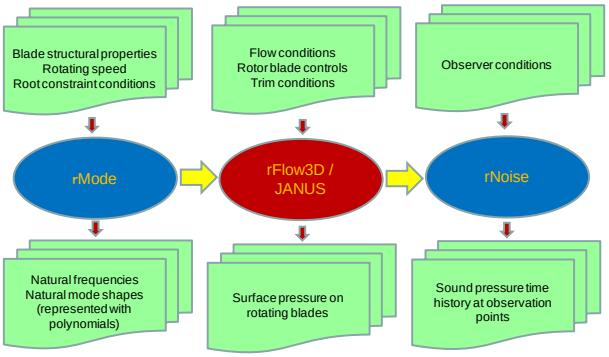

Figure 2: Analysis tool chain for helicopter noise

The converged periodic surface pressure data of one revolution are used to calculate the noise from the rotor. The code *rNoise* considers the elastic motions of the blade when generating the sound source cell position and directions.

Descritions of these three codes are given below.

2.2. Natural frequencies and modes for blade

Based on the Houbolt and Brooks' equations (1)-(3) for a rotating pre-twisted nonuniform blade [5] as shown in Figure 3, we have

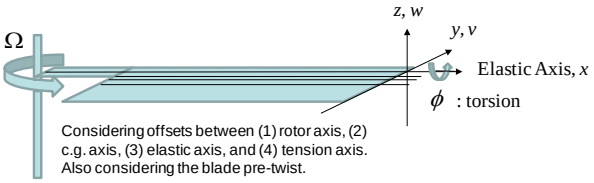

Figure 3: Rotating blade coordinates

Flapwise *w*:

$$
\begin{aligned}
&\left[\left(EI_1\cos^2\beta+EI_2\sin^2\beta\right)w''+\left(EI_2-EI_1\right)\sin\beta\cos\beta v''\right]''\\
&-\left(Tw'\right)'-\left[Te_A\phi\cos\beta+EB_2\beta'\phi'\sin\beta\right]''\\
&-\left(\Omega^2 mre\phi\cos\beta\right)'+m\left(\ddot{w}+e\ddot{\phi}\cos\beta\right)-m\Omega^2 w\sin^2\beta\\
&=L_z+\left(Te_A\sin\beta\right)''+\left(\Omega^2 mre\sin\beta\right)'
\end{aligned}
\tag{1}
$$

Chordwise *v*:

$$
\begin{aligned}
&\left[\left(EI_2-EI_1\right)\sin\beta\cos\beta w''+\left(EI_1\sin^2\beta+EI_2\cos^2\beta\right)v''\right]''\\
&-\left[Te_A\phi\sin\beta+EB_2\beta'\phi'\cos\beta\right]''-\left(Tv'\right)'+m\left(\ddot{v}-e\ddot{\phi}\sin\beta\right)\\
&-\Omega^2 mv\cos^2\beta+\left(\Omega^2 mre\phi\sin\beta\right)'+\Omega^2 me\phi\sin\beta\\
&=L_y+\left(Te_A\cos\beta\right)''+\left(\Omega^2 mre\cos\beta\right)'+\Omega^2 m\left(e_0+e\cos\beta\right)
\end{aligned}
\tag{2}
$$

Torsionwise ϕ:

$$
\begin{aligned}
&-\left\{\left[GJ+Tk_A^2+EB_1(\beta')^2\right]\phi'-EB_2\beta'(v''\cos\beta+w''\sin\beta)\right\}'\\
&+Te_A(v''\sin\beta-w''\cos\beta)+\Omega^2mre(-v'\sin\beta+w'\cos\beta)\\
&+\Omega^2me\sin\beta v+\Omega^2m\left[\left(k_{m2}^2-k_{m1}^2\right)\cos 2\beta+ee_0\cos\beta\right]\phi\\
&+mk_m^2\ddot{\phi}-me(\ddot{v}\sin\beta-\ddot{w}\cos\beta)\\
&=M_x+\left(Tk_A^2\beta'\right)'-\Omega^2m\left[\left(k_{m2}^2-k_{m1}^2\right)\sin\beta\cos\beta+ee_0\sin\beta\right]
\end{aligned}
\tag{3}
$$

Please note Eqs.(2) and (3) are slightly different from those originally in [5] where symmetric small terms for *w* and *v* are retained. It is possible to obtain the full-coupled natural frequencies and corresponding mode shapes based on the equations (1)-(3) with the right-hand forcing terms set to zero. Isakson and Eisley [8] proposed a three-stage transfer matrix method to build-up a [10x10] matrix relating the state variables across a rotating beam element. Unfortunately, non-zero blade cross-section integrals B1 and B2 are required in their formula which often are not available in the publicized data set of the blade structural properties. Murthy [9] proposed an integration transfer matrix method to obtain a relationship between the state variables between the blade tip and the root, but it is reported by Murthy [10] and also noticed by present author that this method does not yield accurate deflections for non-predominant degrees of freedom in a coupled mode shape, the reason being that this approach yields a non-self-adjoint eigenvalue problem even though the original system is self-adjoint. Full-coupled modes were used by present authors with the tension axis offset effects omitted [2] but was found that the accuracy of predicted deformation suffered significantly and the effect of mass axis offset could not be predicted in reasonable trends.

Reliable base mode shapes are crucial to the accuracy of prediction using modal approaches. It is possible to firstly obtain uncoupled torsion modes and a set of coupled bending modes and take into the coupling effects between the bending and torsion in a numerically iterative manner. Moving the terms related to torsion in Eqs.(1) and (2) to the right hand side, then we have

$$
\begin{aligned}
&\left[\left(EI_1\cos^2\beta+EI_2\sin^2\beta\right)w''+\left(EI_2-EI_1\right)\sin\beta\cos\beta v''\right]''\\
&-\left(Tw'\right)'+m\ddot{w}-m\Omega^2w\sin^2\beta\\
&=L_z+\left(Te_A\sin\beta\right)''+\left(\Omega^2mre\sin\beta\right)'\\
&+\left[Te_A\phi\cos\beta+EB_2\beta'\phi'\sin\beta\right]''\\
&+\left(\Omega^2mre\phi\cos\beta\right)'-me\ddot{\phi}\cos\beta
\end{aligned}
\tag{4}
$$

$$
\begin{aligned}
&\left[\left(EI_2-EI_1\right)\sin\beta\cos\beta w''+\left(EI_1\sin^2\beta+EI_2\cos^2\beta\right)v''\right]''\\
&-\left(Tv'\right)'+m\ddot{v}-m\Omega^2v\cos^2\beta\\
&=L_y+\left(Te_A\cos\beta\right)''+\left(\Omega^2mre\cos\beta\right)'+\Omega^2m\left(e_0+e\cos\beta\right)\\
&+\left[Te_A\phi\sin\beta+EB_2\beta'\phi'\cos\beta\right]''\\
&-\left(\Omega^2mre\phi\sin\beta\right)'-\Omega^2me\phi\sin\beta+me\ddot{\phi}\sin\beta
\end{aligned}
\tag{5}
$$

By setting right hand sides of Eqs.(4)-(5) to zero, a set of coupled bending free vibration equations is obtained. The natural frequencies in bending of twisted blades can be calculated using the method given by Isakson and Eisley [11] which is much simpler than the method to obtain the full coupled vibration modes.

And moving the terms related to bending in Eq.(3) to the right hand side, we have

$$
\begin{aligned}
&-\left\{\left[GJ+Tk_A^2+EB_1(\beta')^2\right]\phi'\right\}'\\
&+\Omega^2m\left[\left(k_{m2}^2-k_{m1}^2\right)\cos 2\beta+ee_0\cos\beta\right]\phi+mk_m^2\ddot{\phi}\\
&=M_x+\left(Tk_A^2\beta'\right)'-\Omega^2m\left[\left(k_{m2}^2-k_{m1}^2\right)\sin\beta\cos\beta+ee_0\sin\beta\right]\\
&+\left\{EB_2\beta'(v''\cos\beta+w''\sin\beta)\right\}'-Te_A(v''\sin\beta-w''\cos\beta)\\
&-\Omega^2mre(-v'\sin\beta+w'\cos\beta)-\Omega^2me\sin\beta v\\
&+me(\ddot{v}\sin\beta-\ddot{w}\cos\beta)
\end{aligned}
\tag{6}
$$

The uncoupled torsional free vibration equation is obtained by set the right hand side of Eq.(6) to zero, and the natural frequencies and mode shapes can be calculated by general Myklestad method.

It must be noted that these semi-coupled natural frequencies may be different from those of full coupled analysis, but for conventional high aspect ratio rotor blade where the offsets between elastic axis and mass axis and tension axis are small compared with the blade radius, the difference of natural frequencies between these two approach are considered to be negligible.

A fan-plot of the HART-II [12] blade obtained with this semi-coupled method is shown in Figure 4 where the pitch link stiffness is adjusted to meet the 1st torsion frequency measured experimentally. Coupled bending and uncoupled torsion mode shapes at 100%rpm (1042 RPM) are shown in Figure 5. They are in good agreement with other researchers [13-15].

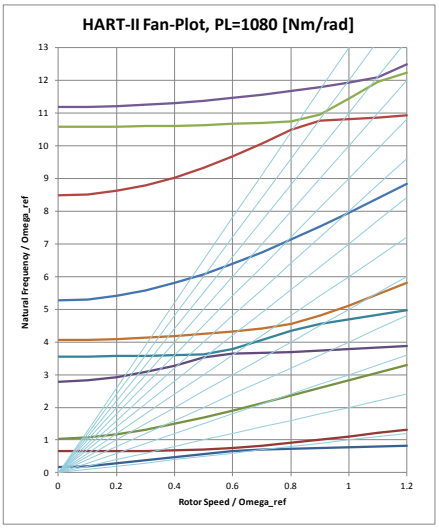

Figure 4: Fan-plot for HART-II rotor blade

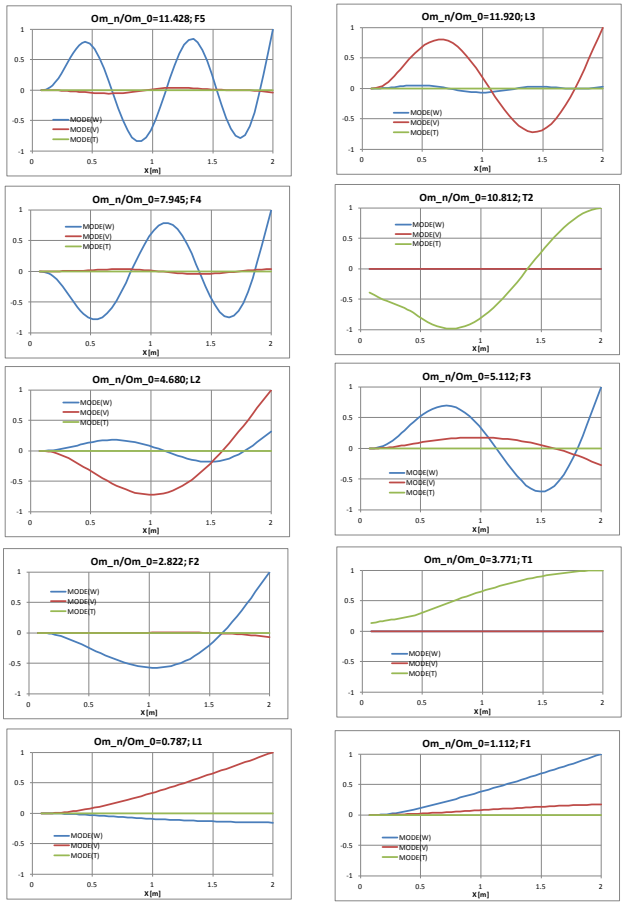

Figure 5: Mode shapes for HART-II blade at 100%rpm

2.3. CFD/CSD/Trim coupling analysis

For BVI calculations, Euler equations in an Arbitrary Lagrangian Eulerian (ALE) form are solved using Finite Volume Method (FVM). The all-speed numerical scheme mSLAU adopted in *rFlow3D* and the moving overlapped grid method are described in detail in [7]. An example of the grid system used with *rFlow3D* code is shown in Figure 6. In Figure 7, the fuselage is in a realistic complex geometry, which is solved with the *JANUS* code [3].

The numerical scheme mSLAU adopted in *rFlow3D* is a modified version of SLAU [16] with extension to the three dimensional moving grid. It is found very suitalbe for the flow around a rotary wing, where the local flow speed varies from very low to transonic. Combining with a Fourth-order Compact MUSCL TVD (FCMT) interpolation method [17] for reconstruction, 4th order spatial accuracy is obtained in the smooth areas which improves the capturing of blade tip vortices. Samples of flowfield results for various flight conditions are shown in Figure 8, where sharp blade tip vortices can be observed.

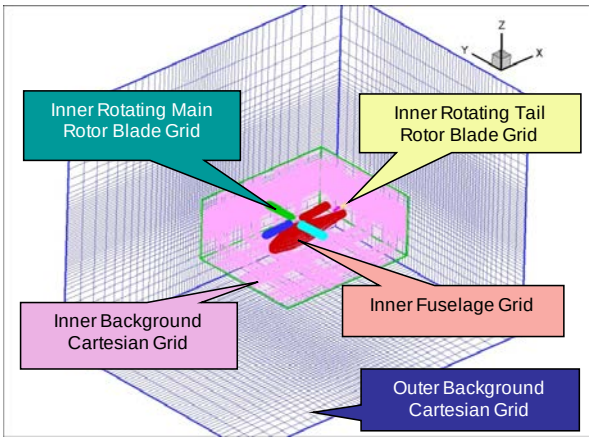

Figure 6: Overlapped grids used in rFlow3D

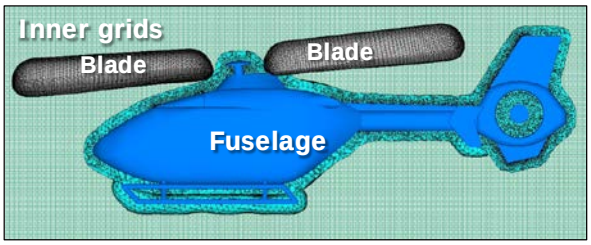

Figure 7: Grid system for JANUS code

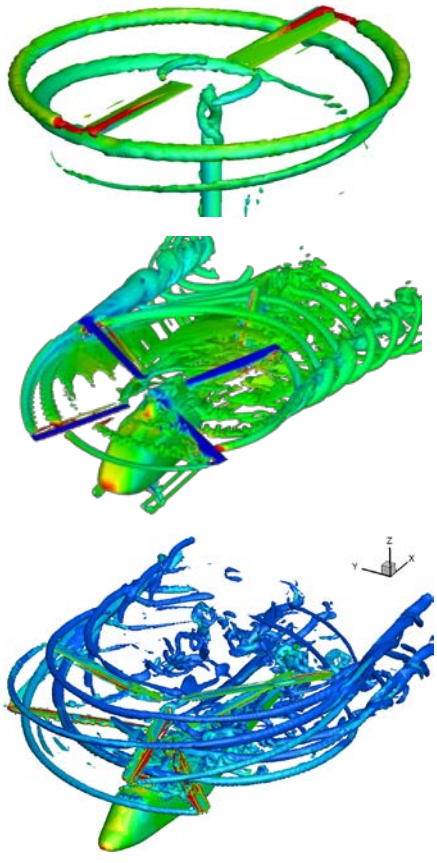

Figure 8: Flowfield around a rotor calculated with mSLAU adopted

The elastic vibrational deformation of the rotor blade is calculated based on the aerodynamic loading obtained with the CFD method.

Following the modified Galerkin procedure, we express the deformation in each direction as a summation of *N* natural modes for bending and *M* natural modes for torsion with time varying amplitudes:

(7) $$w = \sum_{j=1}^{N} q_j w_j$$

(8) $$v = \sum_{j=1}^{N} q_j v_j$$

(9) $$\phi = \sum_{i=1}^{M} p_i \phi_n$$

With orthogonality between natural modes [9], we have,

(10) $$M_n\left(\ddot{q}_n + \omega_n^2 q_n\right) = Q_n$$

where

(11) $$M_n = \int_{r_h}^{R} m\left(w_n^2 + v_n^2\right) dr$$

and

(12)
$$\begin{aligned} Q_n = & \int_{r_h}^{R}\left\{L_z + \left(Te_A \sin\beta\right)'' + \left(\Omega^2 mre \sin\beta\right)'\right\} w_n dr \\ & + \int_{r_h}^{R}\left\{\left[Te_A\phi\cos\beta + EB_2\beta'\phi'\sin\beta\right]'' + \left(\Omega^2 mre\phi\cos\beta\right)' - me\ddot{\phi}\cos\beta\right\} w_n dr \\ & + \int_{r_h}^{R}\left\{L_y + \left(Te_A\cos\beta\right)'' + \left(\Omega^2 mre\cos\beta\right)' + \Omega^2 m\left(e_0 + e\cos\beta\right)\right\} v_n dr \\ & + \int_{r_h}^{R}\left\{\left[Te_A\phi\sin\beta + EB_2\beta'\phi'\cos\beta\right]'' - \left(\Omega^2 mre\phi\sin\beta\right)' - \Omega^2 me\phi\sin\beta + me\ddot{\phi}\sin\beta\right\} v_n dr \end{aligned}$$

for *n*=1,*N*.

Also for torsional mode amplitudes, we have

(13) $$N_i\left(\ddot{p}_i + \mu_i^2 p_i\right) = P_i$$

where

(14) $$N_i = \int_{r_h}^{R} m k_m^2 \phi_i \phi_i dr$$

and

(15)
$$\begin{aligned} P_i = & \int_{r_h}^{R}\left\{M_x + \left(Tk_A^2\beta'\right)' - \Omega^2 m\left[\left(k_{m2}^2 - k_{m1}^2\right)\sin\beta\cos\beta + ee_0\sin\beta\right]\right\}\phi_i dr \\ & + \int_{r_h}^{R}\left\{-\left[EB_2\beta'\left(v''\cos\beta + w''\sin\beta\right)\right]' - Te_A\left(v''\sin\beta - w''\cos\beta\right)\right\}\phi_i dr \\ & + \int_{r_h}^{R}\left\{\Omega^2 mre\left(v'\sin\beta - w'\cos\beta\right) - \Omega^2 mev\sin\beta + me\left(\ddot{v}\sin\beta - \ddot{w}\cos\beta\right)\right\}\phi_i dr \end{aligned}$$

for *i=1,M.*

Notice that torsional deformation terms appears in Eq.(12) and bending terms appear in (15). We can solve Eq.(10) and Eq.(13) together in an iterative manner by using earlier step values of torsion and bending to calculate the generalized force terms. This is equivalent to firstly obtain a semi-coupled solution for bending and uncoupled solution for torsion then take acount the coupling effects between torsion and bending.

Eqs.(10) and (13) can be solved by utilizing the periodicity assumtion of elastic vibrations which leads to solution of a linear equation system in cyclic matrix form. More details can be found in [1]. This periodic amplitude variation for each mode is then approximated with a Fourier series up to 6th harmonics and being used in the CFD calculations.

Also, the rotor pitch angles are adjusted so that the rotor thrust and moments agrees with the target trim rotor values. The aerodynamic loadings used to compute the new elastic deformation are carried out in a loose coupling approach. Trim adjustment and elastic deformation renewal has been done after one revolution of aerodynamic loading is obtained and during the next cycle of CFD calculations, the rotor trim controls and elastic motions are frozen.

The trim adjustment is based on the partial derivatives of the rotor thrust and moments to the rotor controls. The partial derivatives are numerically obtained based on the simple Blade Element Theory where the inflow is uniform and depending on the target thrust only. To improve the computational stability and convergence, the elastic motion changes and the trim adjustment are added with a relaxation factor multiplied.

2.4. Rotor noise prediction

After the converged periodic pressure distributions on the blade surface are obtained, rotor noise at the observing position is calculated using the Farassat Formulation 1 [6] based on Ffowcs Williams-Hawkings equation.

The total noise is composed with the thickness noise and the loading noise as

(16) $$4\pi p'(\mathbf{x},t) = 4\pi\left(p'_T(\mathbf{x},t) + p'_L(\mathbf{x},t)\right)$$

where the thickness noise is

(17) $$4\pi p'_T(\mathbf{x},t) = \frac{\partial}{\partial t}\int_{f=0}\left[\frac{\rho_0 v_n}{r(1-M_r)}\right]_{ret} dS$$

and the loading noise is

(18)
$$4\pi p'_L(\mathbf{x},t) = \frac{1}{c}\frac{\partial}{\partial t}\int_{f=0}\left[\frac{p\cos\theta}{r(1-M_r)}\right]_{ret} dS + \int_{f=0}\left[\frac{p\cos\theta}{r^2(1-M_r)}\right]_{ret} dS$$

The most time consuming part in the noise prediction is to find the source cells that satisfies the retard time criteria and while the blade is rotating and deforming, a lot of coordinate transforming is required. Because the blade rotating, pitching, lead-lagging, flapping and also the elastic deforming are expressed as functions of the azimuth angle, smooth retard time searching is realized. The surface

pressure on the cell surface is interpolated.

3. VALIDATION RESULTS

Validation of the CFD/CSD/Trim/Noise multi-disciplinary analysis chain is separated into two major phases: (1) Utilizing the experimentally measured blade motions, such that the accuracy of airloads and noise prediction can be evaluated. (2) CFD/CSD coupling analysis, so the stand-alone prediction capability can be demonstrated.

Till now, the HART-II International Workshop has provided an excellent opportunity for the CFD/CSD coupling analysis validations under BVI conditions where reliable experimental data for three selected test cases as shown in Table 1 have been released. Many researchers have used HART-II data to validate their predictions till now and an extensive comparative assessment of CFD/CSD coupling methods can be found in [14].

Table 1: HART-II test cases

	BL	MN	MV
M_∞	0.09628	0.09585	0.09563
M_{tip}	0.6387	0.6371	0.6356
μ	0.1508	0.1504	0.1504
C_T	4.63E-03	4.63E-03	4.62E-03
C_{MX}	2.81E-05	4.21E-05	2.81E-05
C_{MY}	-2.81E-05	-4.21E-05	-4.21E-05
θ_0	3.800	3.910	3.800
θ_{1c}	1.917	1.998	2.005
θ_{1s}	-1.342	-1.348	-1.511
θ_{3c}	0	0.405	-0.790
θ_{3s}	0	-0.701	0

For HART-II calculations, two layers of background grid have been used as shown in Figure 9. The grid resolution in inner background has been changed as shown in Table 2. The blade grid size is 121 points in spanwise, 101 points in chordwise and 21 points in bodywise directions. The mesh size in bodywise direction is adjusted according to the resolution in inner background so that sufficient overlapping between the blade grid and inner background grid is secured taking account of the 7 points stencil of the current 4th order scheme adopted. At this stage, only the isolated rotor configuration have been studied compared to experiment. The inclusion of fuselage is expected to improve the prediction in some aspect which will be carried out in the future.

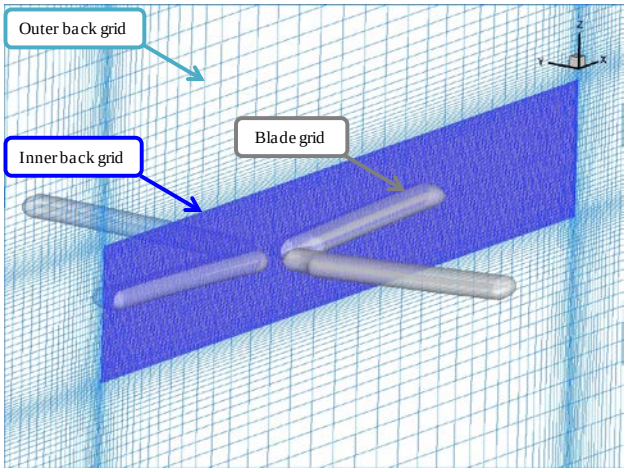

Figure 9: Overlapped grids

Table 2: Inner background grid resolution

Grid Type	X x Y x Z	ΔX= ΔY= ΔZ
Coarse	353x264x138	0.15c
Standard	529x397x207	0.10c
Fine	705x529x275	0.075c

3.1. Prediction of airloads and noise with prescribed blade motions

The accuracies of airloads and trim adjustment together with noise prediction can be evaluated with the blade motions prescribed to the experimentally measured values. As shown in Figure 10, there are certain scatters between blades. Although the airloads are measured mainly on blade 1, averaged blade motions are used in current validation calculations considering the noise generation and BVI phenomenon must take into account of the contributions from all the blades.

The main rotor controls are adjusted to match with the experimental thrust and rotor moments at each loose coupling cycle (every 180 degrees azimuth angle in current studies). As shown in Figure 11, for all the three test cases, collective pitch angle differs from the measurement about 1 degree but showing improvement with grid resolution refinement. About 0.5 degrees are noticed in lateral control pitch angle and the longitudinal pitch angle agrees with the measurement very well. Considering the fuselage is not included in current calculations, the agreement between calculation and measurement is considered satisfactory.

The influence of grid refinement is studied through comparison between the coarse, standard and fine grids. It is crucial to capture and preserve the vortices shedding from the blade tips for accurate simulation of Blade/Vortex Interaction (BVI). The

flowfields of different grid resolution for BL case are visualized with iso-surfaces of Q-criterion as shown in Figure 12. The tip vortices can be observed becoming shaper and stronger with grid refinement. Although non-dissipative preservation of tip vortices may require much denser grids (in order of 10 times from 2D experiences) in the background, it is important to understand to what extent can we accurately simulate the noise level caused by BVI with current computing resources.

Predicted airloads CnM2 are compared at 87%R blade section as shown in Figure 13. While the low frequency variation of CnM2 is not sensitive to grid refinement, at azimuth angle Ψ near 60deg and 300 degrees where the blades pass near the preceding tip vortices, high frequency variations can be observed in the results with standard and fine grid. These high frequency variations can be further identified and directly link to noise generation with its derivative with regard to the azimuth angle. As shown in Figure 14, results of fine grid compares much better with the measurement.

Mid-frequency (6-40 bpf) noise level (BVISPL) distributions on the plane vertically 1.1R below the rotor hub center are shown in Figure 15. The hot spots at the advancing side and retreating side can be indentified from the predictions and the locations compares generally well except for MN case where the hot spot location at the advancing side does not match well with the measurement on coarse and standard grids. Calculation on fine grid for MN case is still on-going. Commonly in all of the predictions, the noise levels on the left-upper corner are heavily over-predicted compared with measurements. Same trend can be seen in other researchers' results [13] also and the reason need to be further investigated.

Maximum BVISPLs at the advancing side hot spots are compared in Figure 16. On fine grids, less than 1 dB accuracy is attained for BL and MV cases. For the relative noise prediction accuracy from the BL case, about 1 dB accuracy is obtained.

3.2. CFD/CSD coupled analysis results

It is concluded from above results that the analysis tools have good airload and noise prediction accuracy with the prescribed experimental elastic motions. To demonstrate the real capability of prediction for blade design, the CFD/CSD coupling analysis have been carried out using the HART-II published blade properties on the standard resolution grids. The natural frequencies and mode shapes at 100%RPM are those shown in Figure 5.

The converged trim controls for CFD/CSD coupling are compared with measurements and also with the results of prescribed motions as shown in Figure 17. Because of the differences in elastic blade motions, which are shown in Figure 18, the trim controls varies within 1 degree to satisfy the trim condition so the predictions give same thrust and rotor moments.

The blade motions at the blade tip predicted by the CFD/CSD coupling analysis agree with measurement well in most aspects, but remarkable differences can be seen as shown in Figure 18. The averages and phases of flap and lag match with measurements fairly well where the amplitudes are slightly under-predicted. The averages of torsion for all three cases are slightly under-predicted about 1 degree which are reflected by the differences in trim collective pitch angles. The amplitudes of torsion for BL and MN case match with measurements well, but for MV case it is significantly under-predicted. The predicted torsion variations for MV and MN cases have a phase lag about 15 degrees. Torsion for BL case shows a peak around Ψ=15 degrees which are not in the measurement and the second peak has a large phase lag about 30 degrees. It must be noted that through numerical experiments it is found the elastic deformations are very sensitive to blade properties especially to the offsets between elastic axis and mass axis and also with the location of tension axis. Considering the scatters between blades in elastic motions, the overall CFD/CSD prediction accuracy can be acceptable. Further improvements and validations of the CSD routines rely heavily on the accuracy in measurement and identification of blade properties.

Airloads predicted with CFD/CSD coupling analysis are shown in Figure 19. The low frequency variations for BL and MV differ from those predicted with prescribed motions. The amplitude is under-predicted in an order of half for MV case which is considered because of the smaller variation of torsion, but for BL and MV cases, the amplitudes of airload variations are predicted excellently.

The airload derivatives are compared in Figure 20, where the variation amplitudes associate with BVI at advancing side for MV case are significantly under-predicted.

The BVISPL plots calculated using the CFD/CSD coupling analysis results are shown in Figure 21. As can be expected from the airload variations, the values at hot spots are under-predicted compared to those of the prescribed motions as indicated in Figure 22.

It can be reasonably explained that the results from the CFD/CSD coupling analysis are less accurate than those with prescribed experimental blade motions. However, most important features are captured through current CFD/CSD coupling analysis which based on the blade design properties and flow conditions only and it can be used in the blade design stages.

4. SUMMARY

An analysis chain from the structural free vibration to CFD/CSD coupling solvers and noise prediction is built for evaluation of the noise reduction effect by active control devices.

Validation with HART-II Workshop data shows good accuracy of airload and noise prediction using prescribed experimental blade motions. The prediction accuracy improves consistently with CFD grid resolution refinement. The maximum BVISPL can be predicted within 1 dB on the fine resolution grids.

For CFD/CSD coupling analysis, reasonable elastic blade motions are obtained based on the blade design properties. The flap and lag motions are predicted with good agreement with measurements. The torsional variations caused by HHC inputs are predicted excellent for MN case, but poor for the MV case. The differences in torsional deformation have significant influence on the airloads. The elastic deformation is very sensitive to blade properties especially the offsets between axes. Further improvements and validations of the CSD routines rely heavily on the accuracy in measurement and identification of blade properties.

ACKNOWLEDGMENTS

The authors are really thankful to the HART-II test team for their generosity to make valuable test data available publicly and especially to Dr. Berend van der Wall, DLR and Dr. Joon Lim, AFDD for their kind supports and management of the HART-II Workshops. Without their enthusiastic efforts, this research and development could take much longer years.

REFERENCES

[1] Tanabe, Y., Saito, S. and Sugawara, H., " Evaluation of Rotor Noise Reduction by Active Devices Using a CFD/CSD Coupling Analysis Tool Chain," 1st Asian Australian Rotorcraft Forum and Exhibition 2012, Busan, Korea, February 12-15, 2012.

[2] Tanabe, Y. and Saito, S., “A Simple CFD/CSD Loose Coupling Approach For Rotor Blade Aeroelasticity,” 33rd European Rotorcraft Forum, Kazan, Russia, September 11-13, 2007. Also JAXA-RR-08-008E, March 2009.

[3] Tanabe, Y., Saito, S., Takayama, O., Sasaki, D. and Nakahashi, K., A New Hybrid Method of Overlapping Structured Grids Combined with Unstructured Fuselage Grids for Rotorcraft Analysis, 36th European Rotorcraft Forum, Paris, France, September 9-11, 2010.

[4] Nakahashi, K., Ito, Y. and Togashi, F., “Some challenges of realistic flow simulations by unstructured grid CFD”, Int. J. for Numerical Methods in Fluids, Vol.43, pp.769-783, 2003.

[5] Houbolt, J.C. and Brooks, G.W., "Differential Equations of Motion for Combined Flapwise Bending, Chordwise Bending, and Torsion of Twisted Nonuniform Rotor Blades," NASA TN-3905, 1957.

[6] Farassat, F., "Derivation of Formulation 1 and 1A of Farassat," NASA TM-2007-214853, 2007.

[7] Tanabe, Y. and Saito, S., “Significance of All-Speed Scheme in Application to Rotorcraft CFD Simulations,” The 3rd International Basic Research Conference on Rotorcraft Technology, Nanjing, China. October, 2009.

[8] Isakson, G. and Eisley, G.J., "Natural Frequencies in coupled bending and torsion of twisted rotating and non-rotating blades," NASA CR-65, 1964.

[9] Murthy, V.R., “Dynamic Characteristics of Rotor Blades”, J. sound & Vibration, vol.49, no.4, pp.483-500, 1976.

[10] Murthy, V.R., “Dynamic Characteristics of Rotor Blades: Integrating Matrix Method,” AIAA J., Vol. 15, No. 4, pp.595-597, April 1977.

[11] Isakson, G. and Eisley, G.J., "Natural Frequencies in bending of twisted rotating and nonrotating blades," NASA TN D-371, 1960.

[12] Yu, Y.H., Tung, C., van der Wall, B., Pausder, H.-J., Burley, C., Brooks, T., Beaumier, P., Delrieux, Y., Mercker, E., & Pengel, K., “The HART-II Test: Rotor Wakes and Aeroacoustics with Higher-Harmonic Pitch Control (HHC) Inputs - The Joint German/French/Dutch/US Project -,” AHS 58th Annual Forum, Montreal, Canada, June 11-13, 2002.

[13] van der Wall, B.G. et. al, "An Assessment of Comprehensive Code Prediction State-of-the-Art Using the HART II International Workshop Data," AHS International 68th Annual Forum & Technology Display, Ft. Worth, TX, May 1-3, 2012.

[14] Smith, M.J., et. al, "An Assessment of CFD/CSD Prediction State-of-the-Art Using the HART II Internaitonal Workshop Data," AHS International 68th Annual Forum & Technology Display, Ft. Worth, TX, May 1-3, 2012.

[15] van der Wall, B.G., "2nd HHC Aeroacoustic Rotor Test (HART II) -Part I: Test Documentation -," DLR Institute Report IB 111-2003/31, 2003.

[16] Shima, E., and Kitamura, K., “On New Simple Low-Dissipation Scheme of AUSM-Family for All Speeds,” 47th AIAA Aerospace Sciences Meeting, Orlando, FA, January 5-8 2009, AIAA Paper 2009-136.

[17] Yamamoto, S. & Daiguji, H., "Higher- Order-Accurate Upwind Schemes for Solving the Compressible Euler and Navier-Stokes Equations," Computers & Fluids, Vol.22, No.2/3, pp.259-270, 1993.

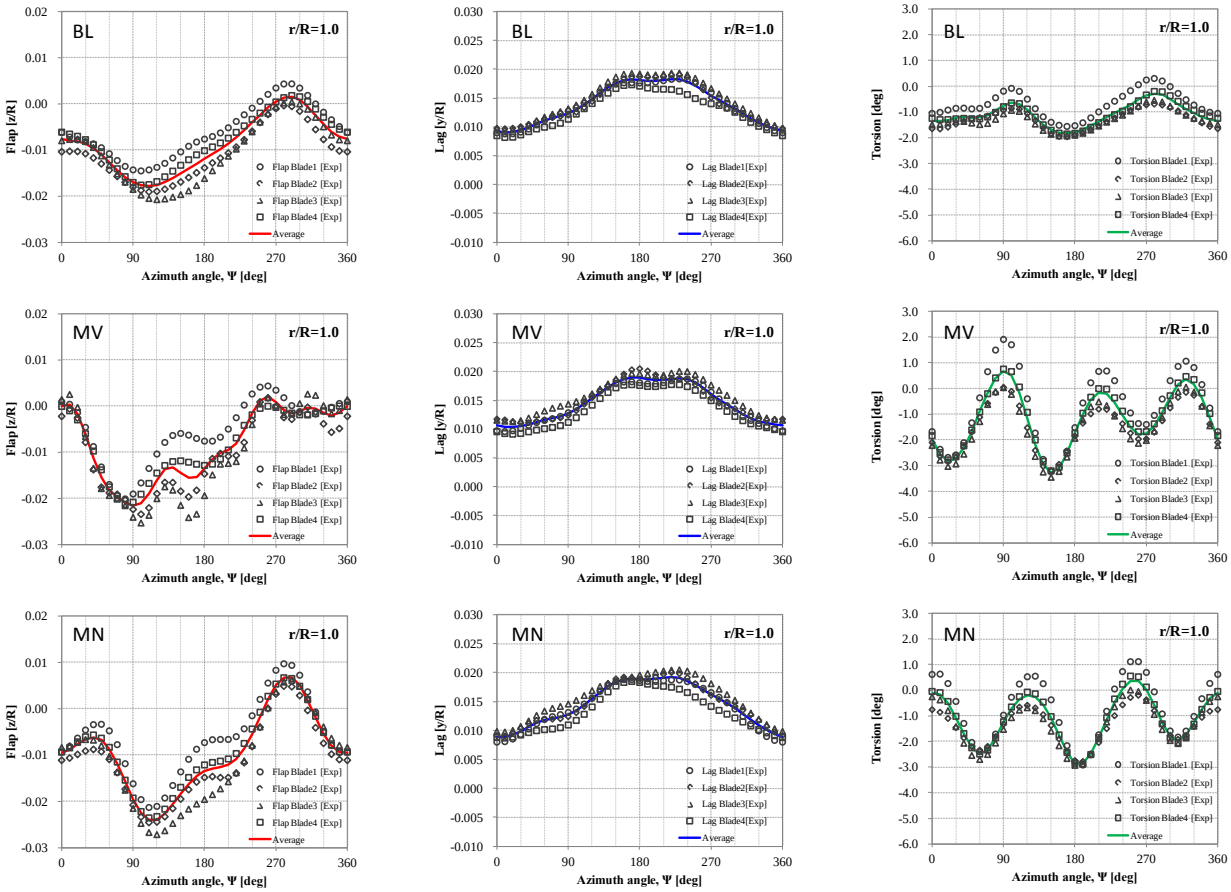

Figure 10: Averaged experimental blade motions

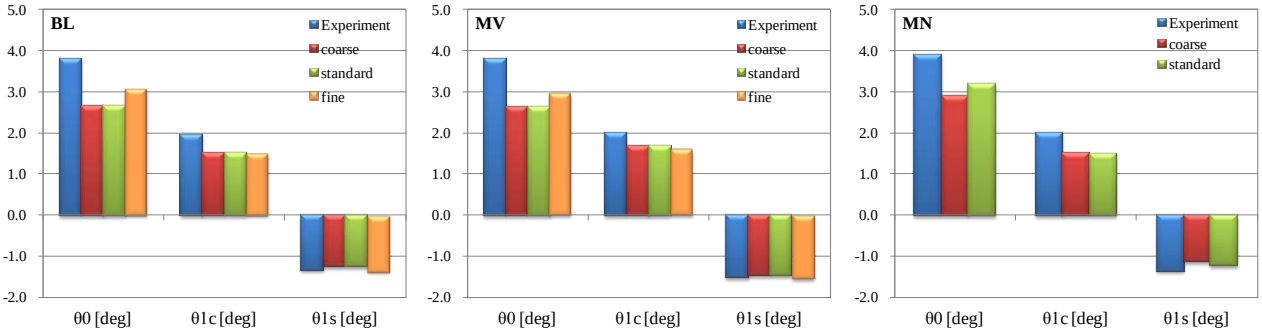

Figure 11: Trim controls

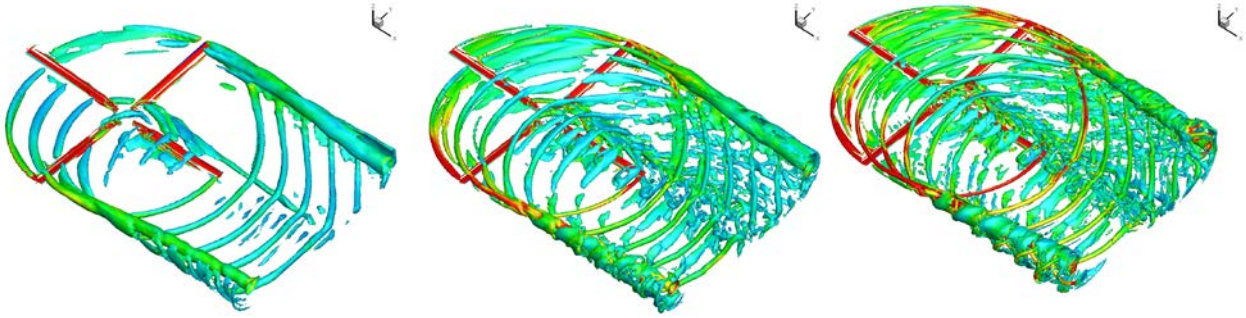

Coarse [0.15c] Standard [0.10c] Fine [0.075c]

Figure 12: Blade tip vortices capturing with grid refinement for BL case

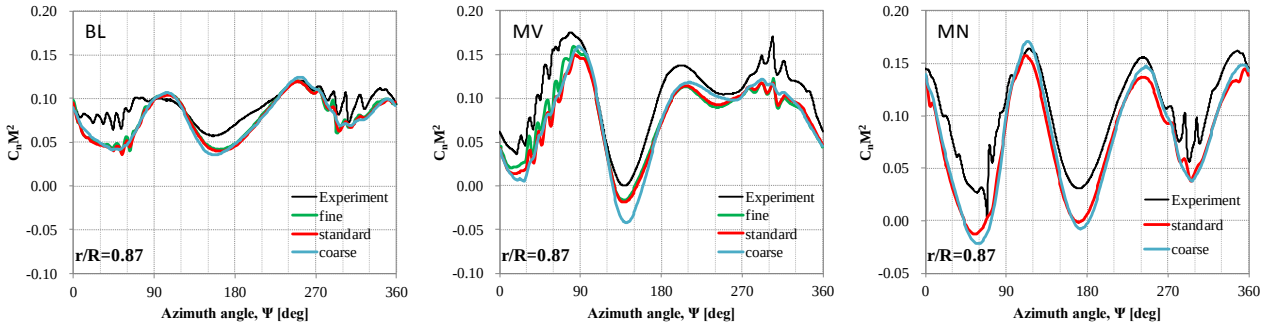

Figure 13: Airloads CnM2 at 87%R

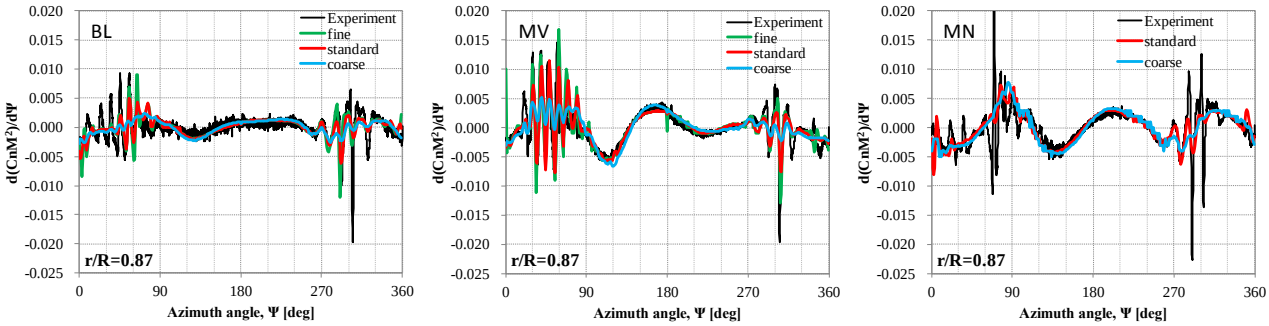

Figure 14: Airload CnM2 derivatives at 87%R

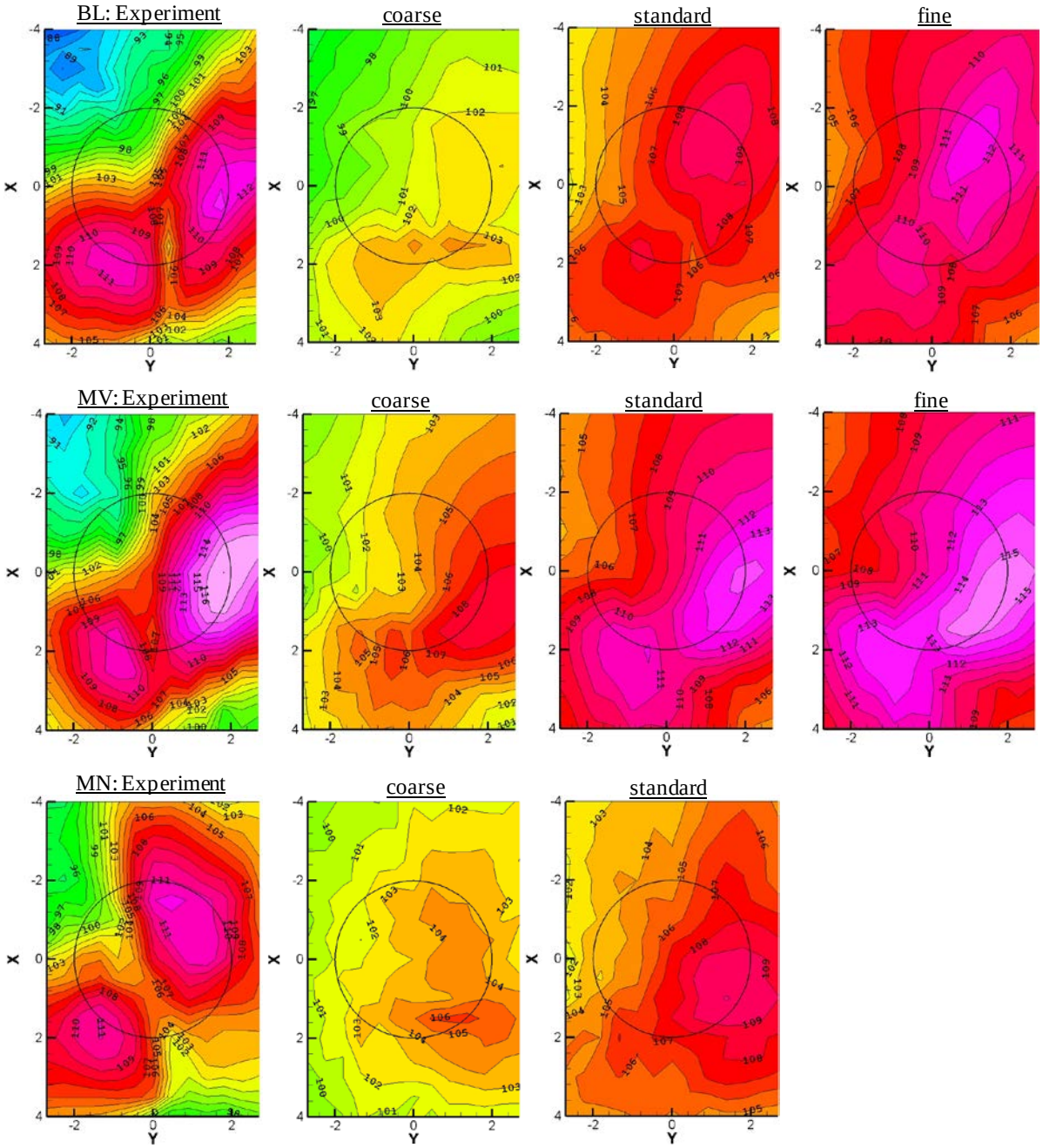

Figure 15: BVISPL carpet plot comparisons

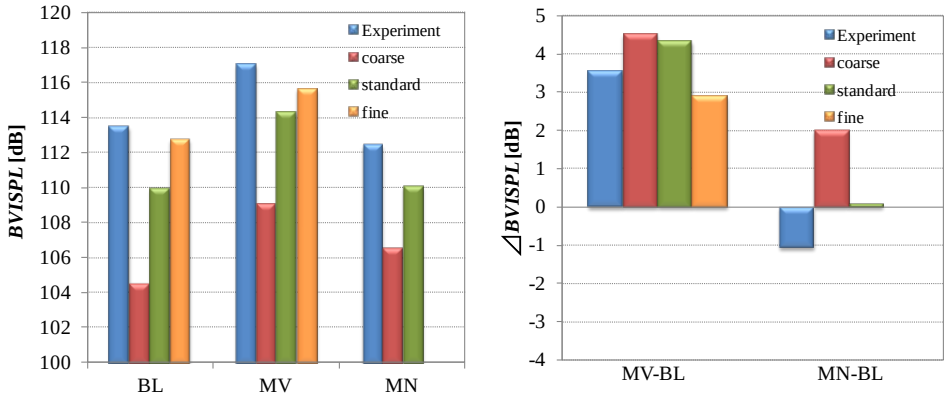

Figure 16: Comparison of Maximum BVISPL (Left) and relative changes (Right)

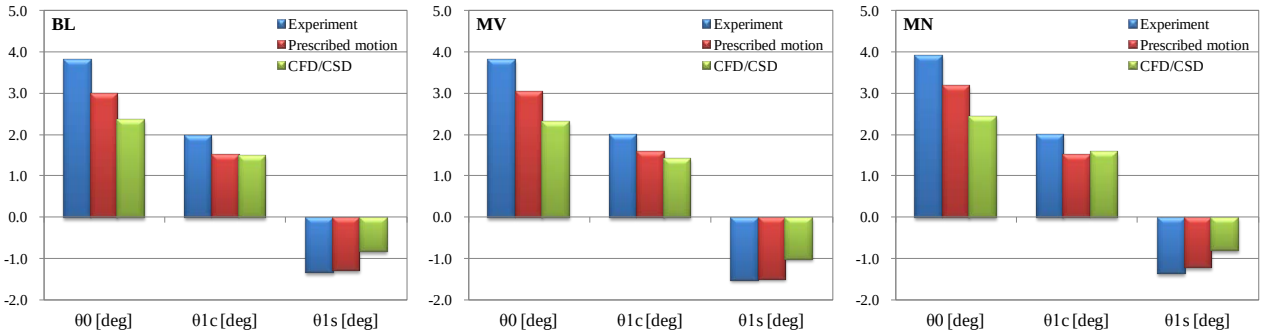

Figure 17: Trim controls for CFD/CSD coupling analysis

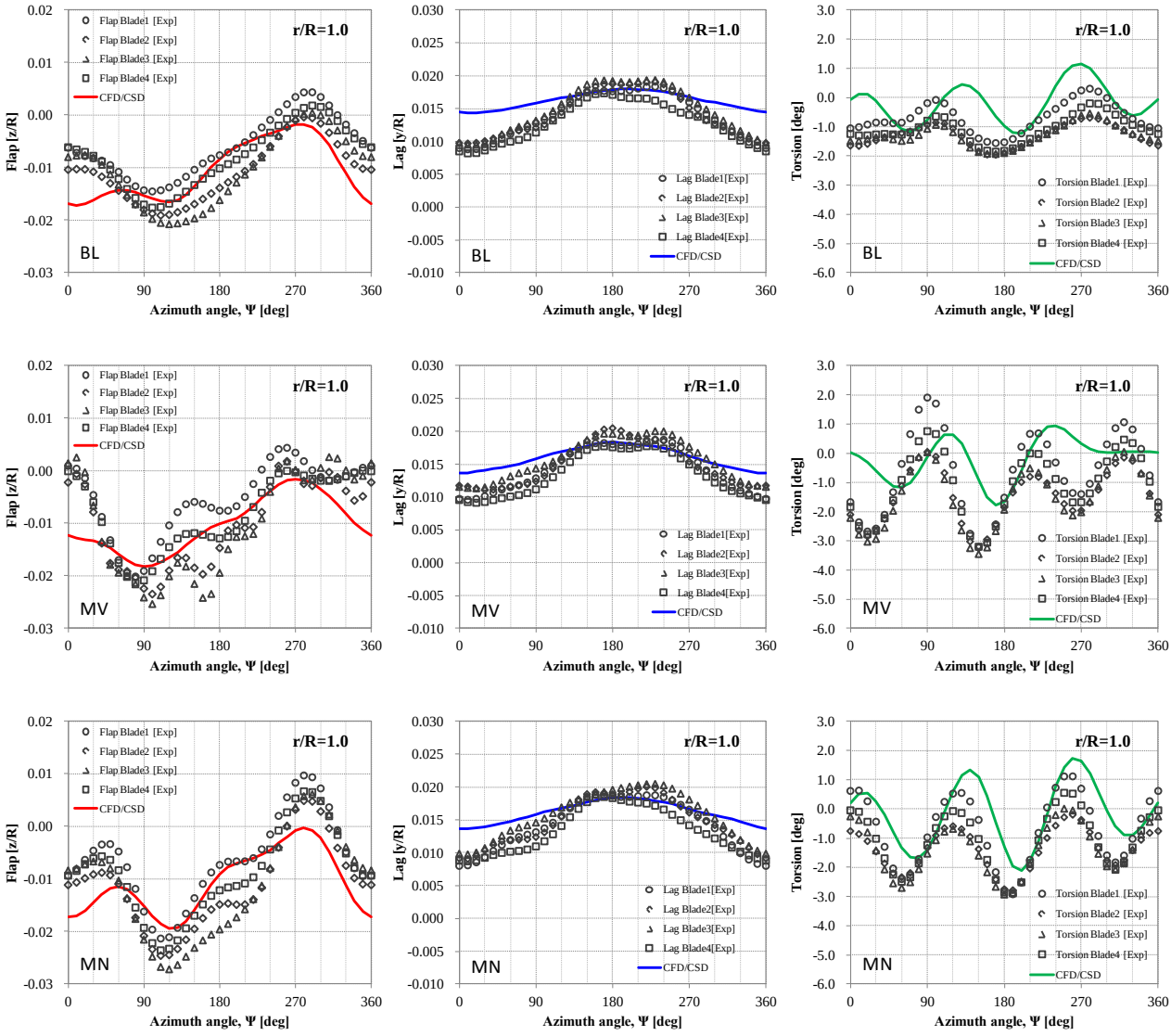

Figure 18: Blade motions obtained through CFD/CSD analysis

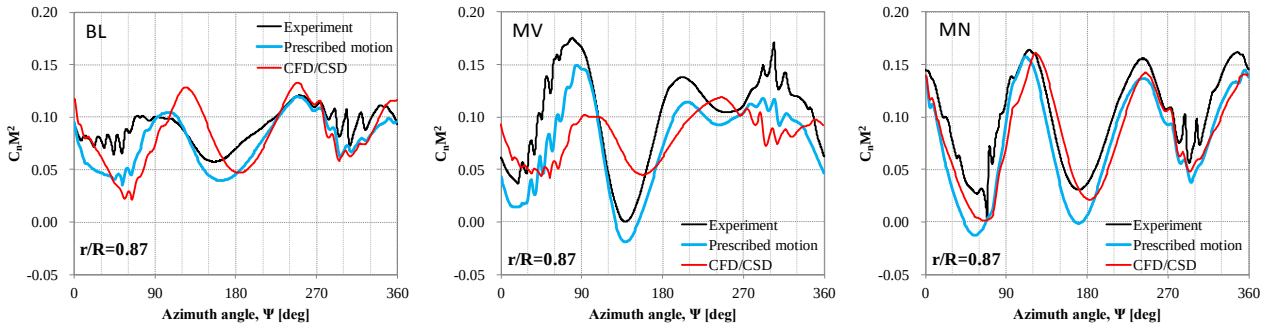

Figure 19: Airloads CnM2 at 87%R predicted with CFD/CSD analysis

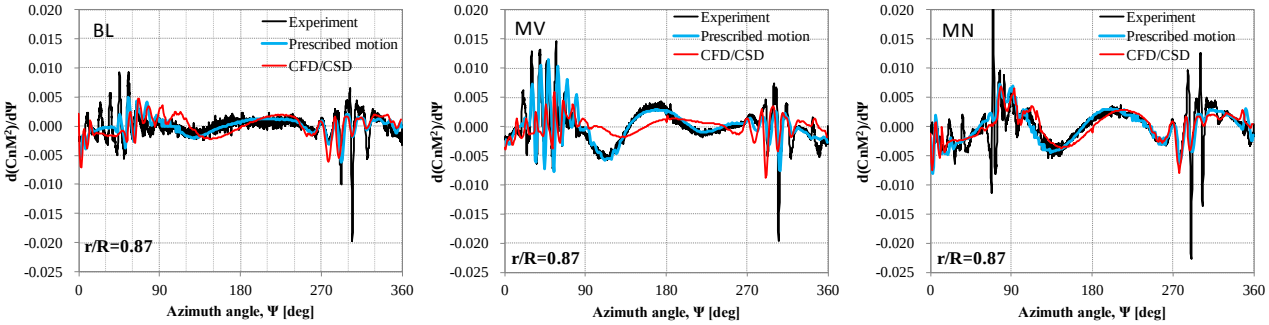

Figure 20: Airload CnM2 derivatives at 87%R predicted with CFD/CSD analysis

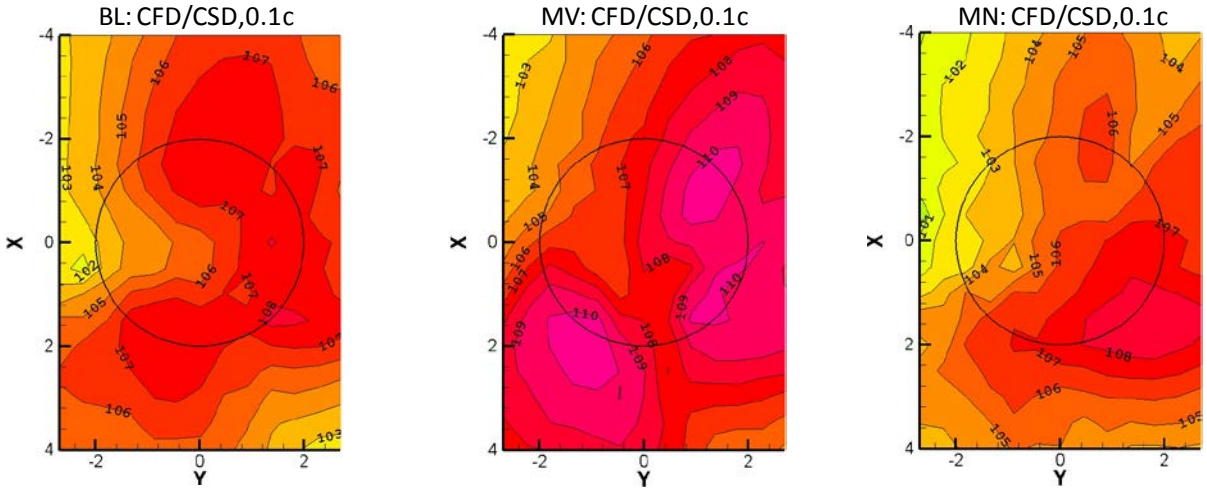

Figure 21: BVISPL carpets from CFD/CSD coupling analysis results

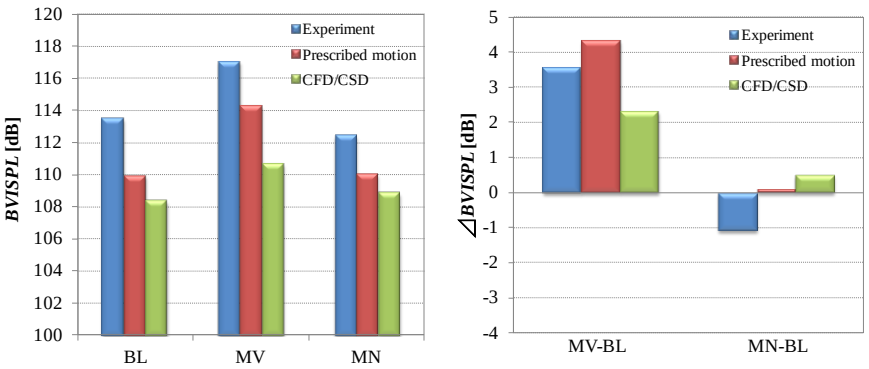

Figure 22: Maximum BVISPL values from CFD/CSD coupling analysis